Journal of Electronics and Electrical Engineering
https://ojs.wiserpub.com/index.php/JEEE/

Article

Cascade Control Applied to a Single-Component Single-Stage Vaporizer—Modeling and Simulation

José M. Campos-Salazar[1,*], Pablo Lecaros[2] and Rodrigo Sandoval[3]

[1]Department of Electronic Engineering, Universitat Politècnica de Catalunya, Barcelona, Spain
[2]Department of Process Engineering, Arauco and Constitution Mill, Concepcion, Chile
[3]Department of Control Engineering, Arauco and Constitution Mill, Concepcion, Chile
E-mail: jose.manuel.campos@upc.edu

Received: 21 July 2023; **Revised:** 23 October 2023; **Accepted:** 24 October 2023

Abstract: This comprehensive research addresses a gap in the literature by providing an extensive examination of a single-component single-stage vaporizer process. The research involves sophisticated analyses such as dynamic modeling, comprehensive control system design and performance evaluation. The study systematically derives a linear state-space model from complex nonlinear dynamic models, laying the basis for the development of two highly effective control systems specifically designed for vaporizer level and temperature control. The simulations of these control structures demonstrate notable properties, including fast disturbance rejection, minimal overshoot, and virtually no steady-state error, emphasizing their robustness and precision. This research focuses on the stability and response of the system and provides insight into its transient behavior during disturbances and setpoint changes. The study's broad implications extend beyond the results and provide a path for future improvements. The results indicate ways to refine the start-up stage, minimize initial overshoot during system initialization, and further improve control strategies. This work has the potential to make a difference in advancing the field of vaporization processes, providing engineers and researchers with the tools and insights needed to improve system reliability and performance in industrial applications.

Keywords: cascade control, FoM, linear equations, mass- and energy-balance, non-linear equations, PI-compensator, simulation, vaporizer

1. Introduction

In industrial plants for the storage and handling of liquid and/or gaseous fuels, it is common to find liquid petroleum gas (LPG) fuels. Boiling systems are used to operate LPGs, which represent one of the most important chemical operations and at the same time the most difficult to operate [1,2]. One of these boiling systems is the vaporization process, where the main equipment is the vaporizer, which is usually built using a pressurized cylindrical tank [1,2].

Usually, the LPG is transported in liquid form at a certain pressure and stored in tanks, the LPG must undergo a phase change from its liquid to its gaseous state, producing the vaporization operation [2]. It is for this reason that these vaporizing systems are necessary.

In order to operate a vaporizer safely while maintaining the product's chemical and thermodynamic properties, it is necessary to have suitable and well-tuned control systems to ensure the correct and safe operation of the relevant process.

DOI: https://doi.org/10.37256/jeee.2220233411

Keeping in mind what is stated in the previous paragraph, it is necessary to have a system of nonlinear or linear equations, which adequately model the vaporizer and then apply to them control design techniques, to finally achieve a controlled model of the process.

It is interesting to note that, in the literature there are a few works and/or papers that address the problem of modeling and control of a vaporizer. For instance, the study in [3], provides an analytical research on the dynamic behavior of polydisperse droplets undergoing evaporation and cooling in a vapor-gas mixture. Based on an analogy with spherical crystal evolution, an analytical theory is developed to understand the interfacial heat and mass transfer kinetics. Key contributions include a dimensionless model, analytical solutions for particle size distribution, temperature differences, and unevaporated mass reduction. However, this study does not address control algorithms or control-related issues, but focuses solely on elucidating the fundamental dynamics of the evaporation-cooling process in droplet systems.

Reference [4] focuses on addressing challenges in the chemical industry through the application of advanced control strategies, specifically model predictive control (MPC), in a vinyl acetate monomer process. The study highlights the limitations of conventional proportional-integral (PI) compensators and the advantages of MPC in dealing with nonlinearity and disturbances. The research attempts to include dynamic analysis, set point tracking, disturbance rejection, and performance comparison with PI control, all focused on the vaporizer unit of the process. The focus of the study is to discuss the potential of MPC in process optimization and control without providing specific equations, algorithms, or diagrams related to the MPC or PI compensator system.

In the study proposed by [5], provides a comprehensive analysis of heat transfer within submerged combustion vaporizers (SCVs) used for liquefied natural gas (LNG) vaporizing. The primary focus is to clarify the complexities of the heat transfer process along with its influencing variables. Through the developed model, accurate calculations of heat transfer coefficients are achieved for both the interior and exterior of the tube, taking into account critical factors such as fluid properties, gas holdup, fouling resistance, and exhaust tube opening ratio. The study analyzes the effect of gas holdup on heat transfer efficiency, highlighting its potential to inhibit optimal heat exchange. In addition, the study explores the effect of exhaust tube opening ratio, highlighting the benefits of higher ratios in enhancing turbulence and mitigating gas holdup. While the study does not address control issues, its findings play a critical role in improving SCV designs, increasing energy efficiency, and fine-tuning LNG vaporization processes. In addition, the study raises awareness of the lack of efforts to model equations and systems to formulate control strategies and frameworks relevant to the vaporizer.

A study focused on improving the efficiency of LNG regasification through advanced strategies within air-heated vaporizers is reported in [6]. In particular, this work provides a unique viewpoint by focusing on heat transfer optimization.

The importance of the study lies in its potential for significant improvements in regasification, cost savings and operational reliability. By exploring green alternatives, clarifying supercritical LNG flow dynamics, and fine-tuning finned tube configurations, this research contributes to greener and more efficient LNG terminals. However, this study does not include control algorithms or control structures related to an LNG process.

The article in [7] refers to a study focused on optimizing high-pressure selective catalytic reduction systems in marine diesel engines to meet stringent emission standards. The research examines several flow guide plate designs within the vaporizer/mixer component to improve the mixing of exhaust gas and urea solution. Specifically, the study identifies irregular trapezoidal plates as the most effective, achieving over 97 % NH_3 concentration uniformity at the outlet while maintaining low pressure drop. It is important to note that the study focuses on thermo-chemical analysis and equation derivation, and does not provide information on control system design or control equation modeling.

The study [8], aims to optimize intermediate fluid vaporizers (IFVs) in a LNG terminal to enhance regasification efficiency, align with market demand, and reduce seawater consumption. To achieve these goals, mathematical modeling of IFV sections, heat transfer coefficient calculations, and determination of parameters like KA values are critical components. The article presents an objective, clear, and concise account of IFV optimization. The results demonstrate how changes in seawater temperature and LNG flow rates affect IFV performance. The study explores the minimum seawater flow rate necessary to prevent freezing and ensure safe operations. It emphasizes the influence of LNG flow rates on NG outlet temperature. Ultimately, an optimization model is created to efficiently configure IFV operations by reducing seawater consumption while still meeting NG volume requirements. These findings provide useful knowledge for LNG terminals to enhance efficiency and environmental sustainability.

Finally, a review of the LNG IFV and its heat transfer characteristics is described in [9]. This article provides a comprehensive overview IFV used in the LNG industry. It examines various aspects of IFVs, including innovative design structures, thermal models, and alternative refrigerants, all aimed at improving heat transfer performance, reducing costs, and improving equipment safety. The paper discusses both subcooled and supercritical LNG vaporization processes, highlighting the significant challenges and opportunities in cryogenic heat transfer. While providing insights from experimental measurements and numerical simulations, it emphasizes the need for further research, particularly in evaluating heat transfer correlations under IFV conditions and conducting cryogenic condensation experiments to optimize IFV operation. This review serves as a valuable resource for engineers and researchers working on LNG vaporization systems, providing a comprehensive understanding of the current state of IFV technology and future directions in this critical field.

The main objective of this article is to address the gap in the literature on state-space modeling and comprehensive control system design for vaporization processes. The introduction provides an overview of this critical gap and emphasizes the significant importance of vaporization systems in different industrial contexts. The system's multifaceted nature highlights the complex interactions between parameters such as liquid level, temperature, and pressure, which require precise control to ensure operational efficiency and stability.

This primer provides a comprehensive perspective on the importance of vaporization systems, with an emphasis on LPG vaporizers in an industrial context. It emphasizes the critical role of well-designed control systems in ensuring safe and efficient operation. In addition, it effectively establishes the need for a mathematical vaporizer model and introduces control design techniques essential to achieving controlled processes.

The introduction properly identifies a gap in the literature regarding the modeling and control of vaporizers. By citing various references [3–9], the introduction effectively establishes the need for this research and positions it as a departure from previous efforts. The references cited strategically highlight the lack of comprehensive studies that include both modeling and control, further emphasizing the relevance of the present study.

However, improving the impact of the introduction could be achieved by increasing clarity in certain sections. Explicitly stating the primary purpose or objective of the study early on would help with clarity. In addition, a concise preview of the study's specific contributions or approach to addressing identified gaps would provide a clearer roadmap for the reader.

While the references to previous work (references [3–9]) contextualize the research, they could be enhanced by emphasizing their direct relevance to the challenges and gaps highlighted in the introduction.

The paper is organized as follows. In sections 2 and 3, the description of the process and the modeling of the system are given, respectively. Then, in sections 4 and 5, the design of the vaporizer control system is developed and simulation results are presented, respectively. Finally, the conclusions are given in section 6.

2. Process Description

The focus of this study is the vaporization system shown in Figure 1. This system consists of a pressurized cylindrical tank provided with two inlet pipes and a single outlet pipe. One of the inlet pipes is connected to the bottom of the tank, while the other is connected to a heating coil. The flow through each inlet pipe is controlled by valves 1 and 2. The heater coil incorporates an inlet and an outlet, where the outlet is connected to a condensate trap labeled T. The primary purpose of this arrangement is to vaporize propane, a specific form of LPG. LPG enters the system through one inlet pipe, while the second inlet pipe introduces a thermal steam flow into the heating coil, effectively facilitating the vaporization process.

The result of this process is the production of vaporized gas, which is exhausted from the tank through the outlet pipe. At the same time, a by-product in the nature of condensed liquid escapes from the outlet of the heating coil and is collected by the condensate trap. The introduction of LPG is characterized by parameters such as flow rate ($f_i(t)$), temperature ($T_i(t)$), pressure ($P_i(t)$), and density (ρ_i). Steam is introduced with its specific flow rate ($w_s(t)$) and pressure ($P_s(t)$). The vaporized gas is discharged from the system at a flow rate ($f_v(t)$).

The whole vaporization process is controlled as described in the section 4. The control system is based on the regulation of the level ($h(t)$), pressure ($P(t)$), and outlet temperature of the heating coil (condensate temperature, $T_s(t)$). Moreover, the vaporizer produces two distinct phases: a liquid- and vapor-phase [1]. The

liquid-phase is identified by properties such as volume ($V(t)$), pressure ($P(t)$), temperature ($T(t)$), and density (ρ). Meanwhile, the vapor-phase is characterized by its volume ($V_v(t)$), pressure ($P_v(t)$), and density (ρ_v).

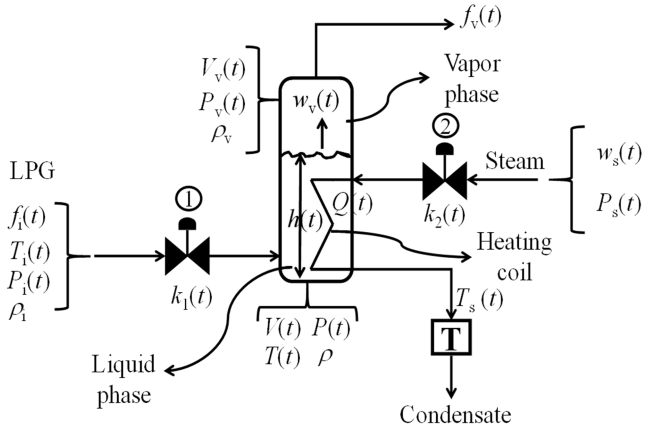

Figure 1. Single-component single-stage vaporizer process.

The theoretical framework assumes homogeneity within the liquid phase of the tank. Heat is added to the system at a rate ($Q(t)$) to achieve the desired pressure value, and consequently the vaporization process is driven at a rate ($w_v(t)$). The assumptions also include the neglect of heat and mass losses through the tank walls and the neglect of dynamic effects from the relatively smaller vapor phase [1]. Table 1 summarizes the variables shown in the process with their engineering units.

Table 1. Summary of Process Variables

Variable	Label
Flow rate of LPG	$f_i(t)$ m³/s
Temperature of LPG	$T_i(t)$ °C
Pressure of LPG	$P_i(t)$ kPa
Density of LPG	ρ_i kg/m³
Mass flow rate of the steam	$w_s(t)$ kg/s
Pressure of the steam	$P_s(t)$ kPa
Flow rate of the output vapor	$f_v(t)$, m³/s
Volume of the liquid phase	$V(t)$ m³
Temperature of the liquid phase	$T(t)$ °C
Pressure of the liquid phase	$P(t)$ kPa
Density of the liquid phase	ρ kg/m³
Volume of the vapor phase	$V_v(t)$ m³
Pressure of the vapor phase	$P_v(t)$ kPa
Density of the vapor phase	ρ_v kg/m³
Condensate temperature	$T_s(t)$ °C
Heat flow	$Q(t)$ kJ/s
Liquid vaporization rate	$W_v(t)$ kg/s
Vaporizer height	$h(t)$ m
Position of valve 1	$k_1(t)$, pu
Position of valve 2	$k_2(t)$, pu

Two control strategies are developed for the correct operation of the vaporizer (details in section 4). Firstly, a single feedback loop controls the vaporizer level, i.e., $h(t)$ by adjusting the position of the valve 1 regarding the variable k_1(t). Keeping a controlled level is essential to prevent potential problems. An excessive perturbation of $f_i(t)$ away from the operating point can lead to overflow and loss of vapor-phase, while a large decrease can empty the vaporizer, causing thermal shock and damage to the heating coil, both of which negatively affect the $w_v(t)$ ratio and the vaporization process [1].

The second strategy takes advantage of a cascade control structure with two feedback loops. The primary loop controls the temperature $T_s(t)$, which indirectly influences the secondary loop, which controls the liquid-phase pressure $P(t)$. This cascade configuration increases control accuracy and robustness, as disturbances affecting the primary loop are effectively compensated by the secondary loop. The manipulation of valve 2, referred to as $k_2(t)$, allows the fine tuning of the vaporization process and the maintenance of optimal conditions even in the presence of external disturbances or variations [2,10,11].

In this context, a potential classification of the system control variables into the designated classifications is shown in Table 2. From Table 2, the measured disturbance variables give special emphasis to the role they play in the vaporizer. In this study, it is assumed that the processes related to the LPG and steam supply are known and constant and are assumed to operate in steady state.

Table 2. Summary of Variables and Functions in Control Structures for Vaporization System

Variable	Label	Control structure	Description
		Manipulated variables	
Position of valve 1	$k_1(t)$	Single feedback loop	Manipulated to control vaporizer height and liquid level
Position of valve 2	$k_2(t)$	Cascade control (inner loop)	Manipulated to regulate pressure of the liquid phase
Pressure of the liquid phase	$P(t)$	Cascade control (outer loop)	Feedback variable within the cascade control structure
		Controlled Variables	
Vaporizer height	$h(t)$	Single feedback loop	Controlled to maintain desired liquid level
Condensate temperature	$T_s(t)$	Cascade control (outer loop)	Controlled to ensure efficient vaporization
Pressure of the liquid phase	$P(t)$	Cascade control (inner loop)	Feedback variable within the cascade control structure
		Measured disturbance variables	
Flow rate of LPG	$f_i(t)$	Both	Measured disturbance affecting vaporization process
Mass flow rate of the steam	$w_s(t)$	Cascade control	Measured disturbance introduced for vaporization
LPG temperature	$T_i(t)$	Both	Measured disturbance potentially impacting vaporization
LPG pressure	$P_i(t)$	Both	Measured disturbance influencing vaporization behavior
		Unmeasured disturbance variables	
Pressure of the steam	$P_s(t)$	Both	Unmeasured disturbance potentially impacting vaporization
		Feedback variables	
Vaporizer height	$h(t)$	Single feedback loop	Feedback variable within the single feedback loop
Pressure of the liquid phase	$P(t)$	Cascade control (inner loop)	Feedback variable within the cascade control structure
Condensate temperature	$T_s(t)$	Cascade control (outer loop)	Feedback variable within the cascade control structure

Also, in this study, the design of the control system for the vaporization process is based on well-defined control specifications and objectives aimed at achieving optimal performance, stability, and operational efficiency within the vaporizer. Both tracking objectives and constraint satisfaction were considered in the formulation of the control strategy. These aspects are listed in Table 3.

Table 3. Detailed Control Specifications for Vaporizer Process

Control aspect	Description
Control objective	Regulate liquid level, vaporization temperature, and internal pressure for efficient vaporization
Control structure	Dual-loop control: single-loop for liquid level, cascade control for level and temperature
Control variables	- Liquid level ($h(t)$): desired steady-state value: 50% - Vaporization temperature ($T_s(t)$): desired steady-state value: 80°C - Internal pressure ($P(t)$): desired steady-state value: 47 kPa
Control actions	Valve positions ($k_1(t)$ and $k_2(t)$): manipulated to control liquid flow and pressure
Control strategy	Minimize overshoots, achieve desired steady-state values, maintain negligible steady-state errors.
Constraints & tracking	Explicit constraints can be defined as: 0 % < $h(t)$ <= 90 % -100 °C < $T_s(t)$ < 400°C 0 kPa < $P(t)$ <= 200 kPa 0 m^3/s <= $f_i(t)$ <= 250 m^3/s 0 kg/s <= $w_s(t)$ <= 250 kg/s 0 pu <= $k_1(t)$ <= 1 pu 0 pu <= $k_2(t)$ <= 1 pu Primary tracking objective: Achieve and maintain desired steady-state values.
Disturbance handling	Respond quickly to disturbances (e.g., changes in vaporization temperature) by adjusting valve positions.

To conclude the description of the process, two critical figures of merit (FoM) are introduced to quantitatively evaluate the efficacy of the proposed control structures. The first FoM focuses on achieving an overshoot rate (OS), of less than 5 % which reflects the degree to which the system response during transient operation goes beyond its steady-state value [2,10,11]. The second FoM is based on achieving a remarkably low steady-state error (SE) of less than 1 %, which emphasizes the accuracy and precision in maintaining desired set points over long periods of operation [2,10,11]. These FoMs provide important measures for evaluating the performance and efficiency of the control structures developed to control the vaporization process efficiently.

3. Process Modeling

The dynamic model of the vaporizer is established based on the fundamental dynamic equations of the liquid-phase, as detailed in [6] and [7]. Assuming equal pressures between the vapor- and liquid-phase ($P(t) = P_v(t)$), the vaporization rate can be defined as $w_v(t) = \rho_v \cdot f_v(t)$, where ρ_v is the vapor phase density and $f_v(t)$ is the vaporized gas flow rate.

The system includes two different balances: a mass balance and two energy balances. Using the mass balance [1,12,13] around the tank a dynamic equation is formulated as follows

$$\frac{\mathrm{d}h(t)}{\mathrm{d}t} = \frac{1}{\pi \cdot \rho \cdot r^2} \cdot \left(\rho_i \cdot f_i(t) - \rho_v \cdot f_v(t)\right) \tag{1}$$

Equation (1) introduces the variable r denotes the radius of the cylindrical tank, in m. By applying an energy balance [1,12,13] around the tank, the resulting expression is defined as follows

$$\begin{aligned} \frac{\mathrm{d}\left(h(t)\cdot T(t)\right)}{\mathrm{d}t} = {} & \frac{\rho_i \cdot C_p}{\pi \cdot r^2 \cdot C_v \cdot \rho} \cdot \frac{f_i(t) \cdot T_i(t)}{h(t)} - \\ & \frac{\rho_v}{\pi \cdot r^2 \cdot C_v \cdot \rho} \cdot f_v(t) \left(C_p \cdot T(t) + \frac{U \cdot A}{\pi \cdot r^2 \cdot C_v \cdot \rho} \cdot \left(T_s(t) - T(t)\right) \right) \end{aligned} \tag{2}$$

Moreover, C_p and C_v denote the heat capacities at constant pressure and volume, respectively, measured in units of kg/m^3. On the other hand, U and A denote the total heat transfer coefficient and the heat transfer area, respectively, in units of W/m^2-°C and m^2.

Given the importance of keeping the tank at the desired pressure (referred to as $P(t)$), the temperature $T(t)$ in (2) needs to be represented as a function of the desired pressure $P(t)$. To achieve this, expression in (3) introduces the equation of state, with the consideration that $P(t)$ can be reasonably assumed to be relatively low [12].

$$\rho = \frac{M}{R} \cdot \frac{P(t)}{T(t)} \tag{3}$$

In this context, the constants M and R are important, since they symbolize the number of moles of the fluid and the ideal gas constant, respectively, both expressed in J/mol-K [1,12]. By substituting (3) into (2), and assuming equal heat capacities ($C_p = C_v = C$), the following equations provide a simplified model that characterizes the dynamics of the vaporization process. Also, from (2) and taking into account that $\mathrm{d}(h(t)\cdot T(t))/\mathrm{d}t = T(t)\cdot(\mathrm{d}h(t)/\mathrm{d}t) + h(t)\cdot(\mathrm{d}T(t)/\mathrm{d}t)$, the energy balance with respect to pressure $P(t)$ can be formulated as follows

$$\begin{aligned} \frac{\mathrm{d}P(t)}{\mathrm{d}t} = {} & \frac{\rho_i \cdot \rho_v \cdot R}{\pi \cdot r^2 \cdot \rho \cdot M} \cdot \frac{f_i(t) \cdot P_i(t)}{h(t)} - \frac{\rho_v \cdot \left(M \cdot C \cdot P(t) + R \cdot \lambda_v\right)}{\pi \cdot r^2 \cdot C \cdot \rho \cdot M} \cdot \frac{f_v(t)}{h(t)} + \\ & \frac{U \cdot A \cdot R \cdot \rho_v}{\pi \cdot r^2 \cdot C \cdot \rho \cdot M} \cdot \frac{T_s(t)}{h(t)} - \frac{U \cdot A}{\pi \cdot r^2 \cdot C \cdot \rho} \cdot \frac{P(t)}{h(t)} - \\ & \frac{\rho_i}{\pi \cdot r^2 \cdot \rho} \cdot \frac{f_i(t) \cdot P(t)}{h(t)} + \frac{\rho_v}{\pi \cdot r^2 \cdot \rho} \cdot \frac{f_v(t) \cdot P(t)}{h(t)} \end{aligned} \tag{4}$$

where λ_v denotes the average heat of vaporization [1,12]. In addition, by applying an energy balance around the heating coil, the resulting expression defined as follows

$$\frac{\mathrm{d}T_s(t)}{\mathrm{d}t} = \frac{\beta}{C_M} \cdot w_s(t) - \frac{U \cdot A}{C_M} \cdot T_s(t) + \frac{U \cdot A}{C_M} \cdot T(t) \tag{5}$$

where, β is the latent heat of condensation in kJ/kg, while C_M is the heat capacity of the heating coil in kJ/°C.

Similar to the previous scenario, it is necessary to express the expression in (5) as a function of $P(t)$. By substituting (3) into (5), the modified version of the energy balance is derived as follows

$$\frac{\mathrm{d}T_s(t)}{\mathrm{d}t} = \frac{\beta}{C_M} \cdot w_s(t) - \frac{U \cdot A}{C_M} \cdot T_s(t) + \frac{U \cdot A \cdot M}{C_M \cdot R \cdot \rho_v} \cdot P(t) \tag{6}$$

The model is completed with additional equations for the control valves. According to [14], LPG can be considered liquid in nature. Therefore, a valve that handles a liquid service is suitable for the service of LPG. Based on this and according to [12,15], the expression that models the dynamics of the LPG flow through the valve 1 can be defined as follows

$$f_{\mathrm{i}}(t)=\frac{C_{\mathrm{v_1}}}{\sqrt{G_{\mathrm{f}}}}\cdot k_1(t)\cdot\sqrt{P_{\mathrm{i}}(t)-\rho\cdot g\cdot h(t)-P(t)} \tag{7}$$

where, C_{v1} is the valve coefficient determined experimentally for each style and size of valve, using water at standard conditions as the test fluid [15]. Also, g represents the gravitational acceleration in m/s².

On the other hand, for steam handling, and according to [12,15], the expression that characterizes valve 2 can be defined as

$$w_{\mathrm{s}}(t)=C_{\mathrm{v_2}}\cdot k_2(t)\cdot\sqrt{P_{\mathrm{s}}(t)\cdot\left(P_{\mathrm{s}}(t)-P(t)\right)} \tag{8}$$

where C_{v2} is also the valve coefficient. Finally, the set of equations composed of (1), (4), and (6)–(8) represents the coupled nonlinear model of the vaporizer.

In order to provide the basis for a feedback-based control system using output linear compensators, a critical step is to linearize the vaporizer model around its equilibrium points (EPs). This involves studying the steady-state behavior of the system to identify these points. By setting the time derivatives of the nonlinear model to zero and replacing the variables with their appropriate steady-state values, denoted by the capital letter and a superscript "ss," the steady-state model is achieved. This key process yields the following expression, as described in [7] and [12].

In the process of determining the EPs, the equations of the nonlinear vaporizer model are set to zero. It should be noted that the set of known and unknown variables in steady state are $\{P_{\mathrm{i}}^{\mathrm{ss}}, P_{\mathrm{s}}^{\mathrm{ss}}, F_{\mathrm{v}}^{\mathrm{ss}}, K_1^{\mathrm{ss}}, K_2^{\mathrm{ss}}; T_{\mathrm{i}}^{\mathrm{ss}}\}$ and $\{H^{\mathrm{ss}}, P^{\mathrm{ss}}, T_{\mathrm{s}}^{\mathrm{ss}}\}$ respectively. This procedure results in the establishment of the steady-state representation of the vaporizer model, defined in (9).

$$\begin{aligned}
&\frac{1}{\pi\cdot\rho\cdot r^2}\cdot\left(\rho_{\mathrm{i}}\cdot F_{\mathrm{i}}^{\mathrm{ss}}-\rho_{\mathrm{v}}\cdot F_{\mathrm{v}}^{\mathrm{ss}}\right)=0\\
&\frac{\rho_{\mathrm{i}}\cdot\rho_{\mathrm{v}}\cdot R}{\pi\cdot r^2\cdot\rho\cdot M}\cdot\frac{F_{\mathrm{i}}^{\mathrm{ss}}\cdot P_{\mathrm{i}}^{\mathrm{ss}}}{H^{\mathrm{ss}}}-\frac{\rho_{\mathrm{v}}\cdot\left(M\cdot C\cdot P+R\cdot\lambda_{\mathrm{v}}\right)}{\pi\cdot r^2\cdot C\cdot\rho\cdot M}\cdot\frac{F_{\mathrm{v}}^{\mathrm{ss}}}{H^{\mathrm{ss}}}+\frac{U\cdot A\cdot R\cdot\rho_{\mathrm{v}}}{\pi\cdot r^2\cdot C\cdot\rho\cdot M}\cdot\frac{T_{\mathrm{s}}^{\mathrm{ss}}}{H^{\mathrm{ss}}}\\
&\frac{U\cdot A}{\pi\cdot r^2\cdot C\cdot\rho}\cdot\frac{P^{\mathrm{ss}}}{H^{\mathrm{ss}}}-\frac{\rho_{\mathrm{i}}}{\pi\cdot r^2\cdot\rho}\cdot\frac{F_{\mathrm{i}}^{\mathrm{ss}}\cdot P^{\mathrm{ss}}}{H^{\mathrm{ss}}}+\frac{\rho_{\mathrm{v}}}{\pi\cdot r^2\cdot\rho}\cdot\frac{F_{\mathrm{v}}^{\mathrm{ss}}\cdot P^{\mathrm{ss}}}{H^{\mathrm{ss}}}=0\\
&\frac{\beta}{C_{\mathrm{M}}}\cdot W_{\mathrm{s}}^{\mathrm{ss}}-\frac{U\cdot A}{C_{\mathrm{M}}}\cdot T_{\mathrm{s}}^{\mathrm{ss}}+\frac{U\cdot A\cdot M}{C_{\mathrm{M}}\cdot R\cdot\rho_{\mathrm{v}}}\cdot P^{\mathrm{ss}}=0\\
&F_{\mathrm{i}}^{\mathrm{ss}}=\frac{C_{\mathrm{v_1}}}{\sqrt{G_{\mathrm{f}}}}\cdot k_1^{\mathrm{ss}}\cdot\sqrt{P_{\mathrm{i}}^{\mathrm{ss}}-\rho\cdot g\cdot H^{\mathrm{ss}}-P^{\mathrm{ss}}}\\
&w^{\mathrm{ss}}=C_{\mathrm{v_2}}\cdot k_2^{\mathrm{ss}}\cdot\sqrt{P_{\mathrm{s}}^{\mathrm{ss}}\cdot\left(P_{\mathrm{s}}^{\mathrm{ss}}-P^{\mathrm{ss}}\right)}
\end{aligned} \tag{9}$$

By replacing the numerical parameters and the steady-state variables of the vaporizer given in Table 4 and Table 5 respectively, and solving the equation system defined in (9), the EPs are calculated and derived as follows: $H^{\mathrm{ss}} \approx 50$ %, $P^{\mathrm{ss}} \approx 18.2$ kPa, and $T_{\mathrm{s}}^{\mathrm{ss}} \approx 55.1$ °C. In accordance with conventional process control practices, liquid levels are often expressed as percentages. Taking this into account and considering the maximum level, denoted as H_{max} (see Table 4), the steady-state value of $h(t)$, i.e., H^{ss} is determined and expressed in percentage format [16]. Moreover, it should be emphasized that the steady-state parameters and variables documented in Table 4 and in Table 5 are derived from different scenarios shown in references [1,12]. These references are valuable sources that provide the essential parameters needed to understand the steady-state characteristics of the system.

For the sake of simplicity in the manipulation of the equations during the linearization process, it is beneficial to reformulate the model in the context of constant parameters. This effort leads to a new nonlinear model of the vaporizer, which is described in (10).

The constants K_s that are included in the model (10) are defined in (11). Formulating the model in this fashion allows for a simpler process of linearization and facilitates subsequent analysis aimed at the design of control systems.

Table 4. Parameters of the Process

Parameters	Value
l_v	0.0387 kg/mol
C	1.68 kJ/kg-K
G_f	1.55
B	2,247 kJ/kg
C_M	504.59 kJ/K
A	22.436 m^2
U	0.303 W/m-°C
G	9.81 m/s^2
r_i	2.01 kg/m^3
r_i	2.05 kg/m^3
r	2.007 kg/m^3
r	2 m
H_{max}	3.5 m
R	0.00831 kJ/mol-K
M	0.0441 mol

Table 5. Steady-State Variables of the process

Variables	Value
P_i^{ss}	300 kPa
P_s^{ss}	106 kPa
F_v^{ss}	10 m^3/s
K_1^{ss}	0.48 pu
K_2^{ss}	0.42 pu
T_i^{ss}	80 °C

$$\begin{cases} \dfrac{\mathrm{d}h(t)}{\mathrm{d}t} = K_{11}\cdot f_i(t) - K_{12}\cdot f_v(t) \\ \dfrac{\mathrm{d}P(t)}{\mathrm{d}t} = K_{21}\cdot\dfrac{f_i(t)\cdot T_i(t)}{h(t)} - K_{22}\cdot\dfrac{f_v(t)}{h(t)} - K_{23}\dfrac{P(t)\cdot f_v(t)}{h(t)} - K_{24}\cdot\dfrac{T_s(t)}{h(t)} \\ \qquad\qquad K_{25}\cdot\dfrac{P(t)}{h(t)} - K_{11}\cdot\dfrac{f_i(t)\cdot P(t)}{h(t)} + K_{12}\dfrac{f_v(t)\cdot P(t)}{h(t)} \\ \dfrac{\mathrm{d}T_s(t)}{\mathrm{d}t} = K_{31}\cdot w_s(t) - K_{32}\cdot T_s(t) + K_{33}\cdot P(t) \\ f_i(t) = K_{41}\cdot k_1(t)\cdot\sqrt{P_i(t) - \rho\cdot g\cdot h(t) - P(t)} \\ w_s(t) = K_{51}\cdot k_2(t)\cdot\sqrt{P_s(t)\cdot\left(P_s(t) - P(t)\right)} \end{cases} \tag{10}$$

$$\begin{cases} K_{11} = \dfrac{\rho_i}{\pi\cdot r^2\cdot\rho}, K_{12} = \dfrac{\rho_v}{\pi\cdot r^2\cdot\rho}, K_{21} = \dfrac{\rho_i\cdot\rho_v\cdot R}{\pi\cdot r^2\cdot\rho}, K_{22} = \dfrac{\rho_v}{\pi\cdot r^2\cdot\rho} \\ K_{23} = \dfrac{\rho_v\cdot R\cdot\lambda_v}{\pi\cdot r^2\cdot C\cdot\rho\cdot M}, K_{24} = \dfrac{U\cdot A\cdot R\cdot\rho_v}{\pi\cdot r^2\cdot C\cdot\rho\cdot M}, K_{25} = \dfrac{U\cdot A}{\pi\cdot r^2\cdot C\cdot\rho} \\ K_{31} = \dfrac{\beta}{C_M}, K_{32} = \dfrac{U\cdot A}{C_M}, K_{33} = \dfrac{U\cdot A\cdot M}{C_M\cdot R\cdot\rho_v}, K_{41} = \dfrac{C_{v_1}}{\sqrt{G_f}}, K_{51} = C_{v_2} \end{cases} \tag{11}$$

Using the techniques of Taylor series expansion and perturbation described in references [10,11,17], the nonlinear model presented in (10) can be linearized. This process yields the linear state-space model, which is briefly expressed as follows

$$\begin{cases} \dot{\mathbf{x}} = \mathbf{A}\cdot\mathbf{x} + \mathbf{B}\cdot\mathbf{u} \\ \mathbf{y} = \mathbf{C}\cdot\mathbf{x} + \mathbf{D}\cdot\mathbf{u} \end{cases} \tag{12}$$

In this model, the vectors representing state, input, and output variables are denoted as **x**, **u**, and **y**, respectively. Specifically, the state vector **x** is defined as $\mathbf{x} = [h(t), P(t), T_s(t)]^T$, the input vector **u** is defined as **u**

= $[f_v(t), P_i(t), P_v(t), T_i(t), k_1(t), k_2(t)]^T$. For this particular scenario, the choice is to equate the output variables to the state variables, thus resulting in $\mathbf{y} = \mathbf{x}$. Symbolically, $\{\mathbf{x}, \mathbf{y}\} \in \{\mathbb{R}^3\}$ and $\mathbf{u} \in \{\mathbb{R}^6\}$. Regarding the assumption $\mathbf{x} = \mathbf{y}$, it should be noted that in a state-space model such as (12), the vector $\mathbf{x}$ and the output vector $\mathbf{y}$ are related, but not necessarily equivalent. In fact, the state vector $\mathbf{x}$ represents the internal state variables of the system, which describe the current state of the system. The output vector $\mathbf{y}$, on the other hand, represents the measurable or observable quantities of interest [10,11,17].

In many cases, the vector $\mathbf{y}$ may be a subset of the vector $\mathbf{x}$, which means that some state variables may correspond to measured outputs [10,11,17]. In this study, the state variables are measured variables of the vaporizer. Therefore, as can be seen, there is a direct relationship between $\mathbf{x}$ and $\mathbf{y}$.

In order to derive the expressions related to the matrices of the model (12), i.e., the state matrix $\mathbf{A}$, the input matrix $\mathbf{B}$, the output matrix $\mathbf{C}$, and the direct-transmission matrix $\mathbf{D}$, the dynamic equations in (10) are first redefined in terms of the g-functions, as is follows

$$
\begin{aligned}
&g_1\left(f_i(t), f_v(t)\right) = K_{11}\cdot f_i(t) - K_{12}\cdot f_v(t)\\
&g_2\left(f_i(t), f_v(t), T_i(t), T_s(t), P(t), h(t)\right) = K_{21}\cdot\frac{f_i(t)\cdot T_i(t)}{h(t)} - K_{22}\cdot\frac{f_v(t)}{h(t)} - K_{23}\frac{P(t)\cdot f_v(t)}{h(t)} - K_{24}\cdot\frac{T_s(t)}{h(t)}\\
&\qquad\qquad - K_{25}\cdot\frac{P(t)}{h(t)} - K_{11}\cdot\frac{f_i(t)\cdot P(t)}{h(t)} + K_{12}\frac{f_v(t)\cdot P(t)}{h(t)}\\
&g_3\left(w_s(t), T_s(t), P(t)\right) = K_{31}\cdot w_s(t) - K_{32}\cdot T_s(t) + K_{33}\cdot P(t)
\end{aligned}
\tag{13}
$$

$$
\mathbf{A} = \frac{\partial \mathbf{g}}{\partial \mathbf{x}}\bigg|_{\mathbf{Q}^{ss}} = \begin{bmatrix} \frac{\partial g_1}{\partial h(t)} & \frac{\partial g_1}{\partial P(t)} & \frac{\partial g_1}{\partial T_s(t)} \\ \frac{\partial g_2}{\partial h(t)} & \frac{\partial g_2}{\partial P(t)} & \frac{\partial g_2}{\partial T_s(t)} \\ \frac{\partial g_3}{\partial h(t)} & \frac{\partial g_3}{\partial P(t)} & \frac{\partial g_3}{\partial T_s(t)} \end{bmatrix}_{\mathbf{Q}^{ss}}
$$

$$
\mathbf{B} = \frac{\partial \mathbf{g}}{\partial \mathbf{u}}\bigg|_{\mathbf{Q}^{ss}} = \begin{bmatrix} \frac{\partial g_1}{\partial f_v(t)} & \frac{\partial g_1}{\partial P_i(t)} & \frac{\partial g_1}{\partial P_v(t)} & \frac{\partial g_1}{\partial T_i(t)} & \frac{\partial g_1}{\partial k_1(t)} & \frac{\partial g_1}{\partial k_2(t)} \\ \frac{\partial g_2}{\partial f_v(t)} & \frac{\partial g_2}{\partial P_i(t)} & \frac{\partial g_2}{\partial P_v(t)} & \frac{\partial g_2}{\partial T_i(t)} & \frac{\partial g_2}{\partial k_1(t)} & \frac{\partial g_2}{\partial k_2(t)} \\ \frac{\partial g_3}{\partial f_v(t)} & \frac{\partial g_2}{\partial P_i(t)} & \frac{\partial g_2}{\partial P_v(t)} & \frac{\partial g_2}{\partial T_i(t)} & \frac{\partial g_2}{\partial k_1(t)} & \frac{\partial g_2}{\partial k_2(t)} \end{bmatrix}_{\mathbf{Q}^{ss}}
$$

$$
\mathbf{C} = \frac{\partial \mathbf{y}}{\partial \mathbf{x}}\bigg|_{\mathbf{Q}^{ss}} = \begin{bmatrix} \frac{\partial h(t)}{\partial h(t)} & \frac{\partial h(t)}{\partial P(t)} & \frac{\partial h(t)}{\partial T_s(t)} \\ \frac{\partial P(t)}{\partial h(t)} & \frac{\partial P(t)}{\partial P(t)} & \frac{\partial P(t)}{\partial T_s(t)} \\ \frac{\partial T_s(t)}{\partial h(t)} & \frac{\partial T_s(t)}{\partial P(t)} & \frac{\partial T_s(t)}{\partial T_s(t)} \end{bmatrix}_{\mathbf{Q}^{ss}} = \mathbf{I}_{3\times 3}
$$

$$
\mathbf{D} = \frac{\partial \mathbf{y}}{\partial \mathbf{u}}\bigg|_{\mathbf{Q}^{ss}} = \begin{bmatrix} \frac{\partial h(t)}{\partial f_v(t)} & \frac{\partial h(t)}{\partial P_i(t)} & \frac{\partial h(t)}{\partial P_v(t)} & \frac{\partial h(t)}{\partial T_i(t)} & \frac{\partial h(t)}{\partial k_1(t)} & \frac{\partial h(t)}{\partial k_2(t)} \\ \frac{\partial P(t)}{\partial f_v(t)} & \frac{\partial P(t)}{\partial P_i(t)} & \frac{\partial P(t)}{\partial P_v(t)} & \frac{\partial P(t)}{\partial T_i(t)} & \frac{\partial P(t)}{\partial k_1(t)} & \frac{\partial P(t)}{\partial k_2(t)} \\ \frac{\partial T_s(t)}{\partial f_v(t)} & \frac{\partial T_s(t)}{\partial P_i(t)} & \frac{\partial T_s(t)}{\partial P_v(t)} & \frac{\partial T_s(t)}{\partial T_i(t)} & \frac{\partial T_s(t)}{\partial k_1(t)} & \frac{\partial T_s(t)}{\partial k_2(t)} \end{bmatrix}_{\mathbf{Q}^{ss}} = \mathbf{0}_{3\times 6}
$$

(14)

Then the vector function $\mathbf{g}$ is defined as $\mathbf{g} = [g_1(f_i(t), f_v(t)), g_2(f_i(t), f_v(t), T_i(t), T_s(t), P(t), h(t)), g_3(w_s(t), T_s(t), P(t))]^T$, where $\mathbf{g} \in \{\mathbb{R}^3\}$. Finally, taking into account $\mathbf{g}$, $\mathbf{x}$, $\mathbf{u}$, and $\mathbf{y}$, the matrices $\mathbf{A}$, $\mathbf{B}$, $\mathbf{C}$, and $\mathbf{D}$ are defined in (14). From (14), $\mathbf{Q}^{ss}$ is the vector of equilibrium points defined as $\mathbf{Q}^{ss} = [H^{ss}, P^{ss}, T_s^{ss}]$, where $\mathbf{Q}^{ss} \in \{\mathbb{R}^3\}$. Also, the functions g_j, denoted by $j \in \{1, 2, 3, 4\}$, have been intentionally presented in (14) without explicitly

including the time dependence of their component variables. This omission improves the clarity and readability of the (14). Moreover, the matrices $\mathbf{I}_{3x3}$ and $\mathbf{0}_{3x6}$ are the identity and zero matrices of dimension 3x3 and 3x6 respectively. Symbolically, $\{\mathbf{A}, \mathbf{C}\} \in \mathscr{M}_{3x3}\ \{\mathbb{R}\}$ and $\{\mathbf{B}, \mathbf{D}\} \in \mathscr{M}_{3x6}\ \{\mathbb{R}\}$.

It should be noted that the Jacobians (equation (14)) play a key role in calculating the **A**, **B**, **C**, and **D** matrices for the linear state-space model. These matrices describe the system's dynamic behavior, input-output relationships, and interactions [10,11,17]. The Jacobian matrix $\partial\mathbf{g}/\partial\mathbf{x}$, evaluated at the equilibrium points grouped in $\mathbf{Q}^{ss}$, provides the matrix **A**, which represents the state transitions [10,11,17]. Similarly, the Jacobian matrix $\partial\mathbf{g}/\partial\mathbf{u}$, also at $\mathbf{Q}^{ss}$, builds matrix **B**, reflecting input influences on the system [10,11,17]. Matrix **C**, which describes output relations, is derived from the Jacobian matrix $\partial\mathbf{y}/\partial\mathbf{x}$ evaluated at $\mathbf{Q}^{ss}$. This indicates how changes in state variables affect the output of the system. Finally, the **D** matrix, representing direct transmission, is derived from the Jacobian matrix $\partial\mathbf{y}/\partial\mathbf{u}$, again at $\mathbf{Q}^{ss}$. It shows how changes in the inputs directly affect the outputs [10,11,17].

An important technical consideration arises when dealing with the derivation of the Jacobians in (14). This procedure requires a generalized format, since, in this case, the application of the Jacobians depends on the evaluation of the g-functions. In particular, this approach avoids the generation of long expressions that arise when Jacobians are evaluated based on the *g*-functions.

The section covers the dynamic modeling of a vaporization system, emphasizing equations that describe mass and energy balances. An equation of state linking pressure, temperature, and density is introduced. Control valve dynamics are discussed for both liquid and vapor services. The nonlinear model is established using g-functions, setting the stage for linearization. The importance of Jacobian matrices is emphasized in the derivation of **A**, **B**, **C**, and **D** for the linear state-space model. Equating state and output variables is justified, simplifying the model. Overall, this section provides a thorough exploration of vaporization system dynamics.

4. Control System Design

As discussed in the previous sections of this article, the control system designed for the vaporizer was selected using two control structures. A single-loop structure and a cascade control-loop structure. The proposed control system is shown in Figure 2. The use of a single-loop structure and a cascade-loop control strategy in the proposed vaporizer process control system is based on a detailed analysis of the system dynamics and control goals (section 2 and section 3).

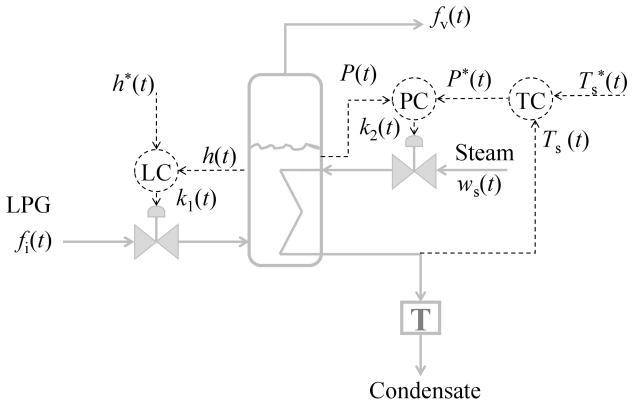

Figure 2. This figure shows the control structure of the vaporizer with two loops: a level control loop with a level compensator (LC) and a cascade control structure with a temperature compensator (TC) and a pressure compensator (PC). Both loops use control valves to effectively regulate temperature, pressure and liquid level. This integration increases system efficiency and ensures optimum operation.

The choice of a single-loop control structure for level control, as shown in Figure 2, is based on the need to maintain a constant $h(t)$ within the vaporizer. By using valve 1 and its manipulating variable $k_1(t)$, this approach focuses the control objective on maintaining $h(t)$ only. This emphasis allows the system to effectively deal with fluctuations in liquid flow rates and disturbances that directly affect the liquid level. This focused approach simplifies the control process, mitigates the potential for cross-variable disturbances, and establishes a robust and rapid $h(t)$ control mechanism, thereby improving overall stability and reliability [10,11,17,18].

On the other hand, and according to Figure 2, the choice of a cascade-loop control structure for temperature ($T_s(t)$) and pressure ($P(t)$) regulation takes into account the complex relationship between these variables and their influence on vaporization efficiency. Temperature control within the vaporizer is closely related to the pressure of the liquid-phase. The cascade structure provides a good solution to address this coupling. The external temperature compensator (TC) focuses on precise temperature control, generating a reference pressure ($P^*(t)$) that optimizes temperature control by adjusting the pressure by manipulating valve 2, i.e., $k_2(t)$. The internal pressure compensator (PC) then provides precise pressure control by fine-tuning the position of valve 2. This hierarchical approach addresses the fact that effective temperature control requires dynamic pressure adjustments, resulting in improved process efficiency and stability [10,11,17].

The combined use of these two control structures provides a balanced and comprehensive approach. The single-loop design provides direct and reliable control of the critical liquid level, ensuring consistent operation. At the same time, the cascade loop configuration handles the complex interaction between temperature and pressure to improve overall control performance and adaptability. This dual strategy uses the benefits of each approach to effectively address the process complexities of the vaporizer, resulting in enhanced stability, efficiency, and reaction time in real-world operating scenarios.

The study of the control system's process plants requires a transformation of the linear model expressed in (12) from its time domain to the Laplace domain (s-domain), which is achieved by applying the Laplace transform. As described in [12] and [11], the model initially defined in (12) is transformed to the s-domain, yielding the following expression:

$$\frac{\mathbf{Y}(s)}{\mathbf{U}(s)} = \mathbf{C} \cdot \left(s \cdot \mathbf{I} - \mathbf{A} \right)^{-1} \cdot \mathbf{B} + \mathbf{D} \tag{15}$$

This equation, (15), incorporates a set of transfer functions (TFs) that closely represent the behavior of the system in the Laplace domain.

In (15), the identity matrix $\mathbf{I}$ shares equivalent dimensions with the matrix $\mathbf{A}$, i.e., $\mathbf{I}_{3x3}$. Due to the complexity of the multi-variable process, equation (15) includes a set of 18 TFs that together build the linear model within the Laplace domain, customized to the specifics of the vaporizer process under study. The vectors $\mathbf{Y}(s)$ and $\mathbf{U}(s)$ are characterized as $\mathbf{Y}(s) = [H(s), P(s), T_s(s)]^T$ and $\mathbf{U}(s) = [P_i(s), P_s(s), K_1(s), K_2(s), F_v(s), T_i(s)]^T$, respectively. It is worth noting that $\mathbf{Y}(s) \in \{\mathbb{C}^3\}$, while $\mathbf{U}(s) \in \{\mathbb{C}^6\}$.

Given the large of the s-domain expressions derived from (15), a practical approach is taken to simplify the analysis. Each of the TFs is redefined using the established principle of superposition. This redefinition is expressed as $G_{ij}(s) = \mathbf{Y}(1, i)/\mathbf{U}(1, j)$, where $i \in \{1, 2, 3\}$ representing the output variables $\{H(s), P(s), T_s(s)\}$ and $j \in \{1, 2, 3, 4, 5, 6\}$ denoting the input variables $\{P_i(s), P_s(s), K_1(s), K_2(s), F_v(s), T_i(s)\}$.

From the information given in (15) and according to the TFs defined in $G_{ij}(s)$, a block diagram of the linear model in (12) can be determined in the s-domain. The s-domain model is shown in Figure 3.

After calculating the TFs and establishing the linear s-domain model of the vaporizer, the next task is to design the compensators that are essential for the operation of the system. In this context, linear feedback output compensators, specifically of the proportional-integral (PI) type, are selected for implementation. This choice is influenced by the extensive literature supporting the use of PI compensators in industrial systems. The benefits of using PI compensators are widely recognized, as evidenced by numerous articles discussing their effectiveness in improving system performance and control.

For instance, the article reported by [19], explores several applications of proportion-integral-derivative compensators and highlights their effectiveness in areas such as dc motor control, power system stability, automatic voltage regulation, controlled dc drives, time delay compensation, load frequency problems, and stability improvement. Specifically, PI compensators offer benefits such as improved stability and steady-state accuracy in load frequency control, precise time delay compensation, fast response and stability in adjusting-voltage regulators systems, accurate speed and torque control in dc motor control. However, careful tuning is critical to optimize performance and prevent transient overshoot. Overall, PI compensators play a key role in improving control processes in these applications.

The study in [20], discusses the application of PI compensators in several systems, highlighting their importance in achieving stability, improved performance, and effective control. The article discusses the use of PI compensators in systems such as robotic manipulators, industrial processes, and thermal plants. The benefits of using PI compensators include improved tracking accuracy, reduced steady-state error, and robust performance.

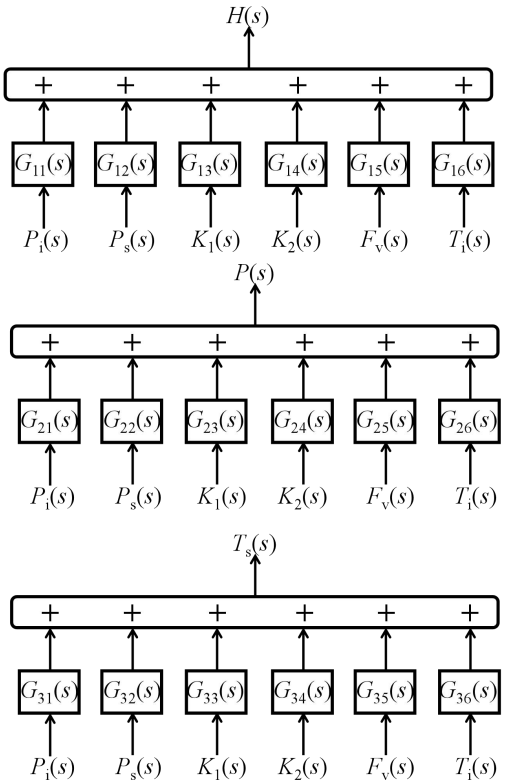

Figure 3. The block diagram of the vaporizer process represents its overall structure. The multivariable nature of the system is evident from the presence of 6 transfer functions per system output. This indicates that there are multiple input-output relationships that need to be considered in the control design and analysis of the vaporizer.

These compensators contribute to precise position control in robotic systems, precise control of industrial processes, and temperature control in thermal plants. However, it is important to carefully tune the compensator parameters to match the system characteristics and avoid problems such as overshooting. In summary, PI compensators play an important role in improving the performance and stability of control systems in a wide range of applications.

Reference [21] is a study that analyzes control strategies for a complex chemical process involving a reactor, flash tank, and recycle tank. The application and performance of PI control, dynamic matrix control (DMC), and generic model control (GMC) are examined through simulation. The process dynamics are represented by differential equations. The study compares these control methods for set point tracking and disturbance rejection. DMC emerges as the superior option, showing faster settling time and improved control performance compared to PI and GMC. This study emphasizes the importance of parameter tuning and control strategies for effective process control. This article also identifies some advantages of using a PI compensator. This compensator offers several advantages in industrial control applications. It is a fundamental and widely used control strategy due to its simplicity and robustness. PI control provides stability and steady-state accuracy for several processes. It is easy to implement and does not require complex calculations, making it suitable for real-time control systems. The integral action of the PI compensator helps eliminate steady-state errors and adapt to changes in set points or disturbances. PI compensators are effective for controlling processes with predictable behavior and minimal interactions. In addition, PI compensators are relatively easy to tune, making them suitable for a wide range of control tasks and industries.

From the information extracted in [19–21] and taking into account [10,11,17], it can be seen that choosing PI compensators over other control strategies is a reasoned decision based on a thorough evaluation of the benefits and drawbacks, taking into account the specific characteristics of the vaporizer process and the desired control objectives. A comprehensive analysis can be done as follow:

- Benefits of PI compensators
  1) Steady-state and transient performance: PI compensators provide accurate steady-state control and robust transient response. In the vaporizer process, maintaining precise temperature, pressure, and liquid levels is essential for efficiency. The integral action of PI compensators eliminates steady-state

errors and ensures prompt disturbance rejection, thus achieving desired operating conditions effectively.

2) Integral action for disturbance rejection: Vaporizer processes are often subject to disturbances such as varying liquid flow rates or external temperature changes. The integral term in PI compensators provides effective compensation for these disturbances by continuously adjusting the control effort based on the accumulated error. This integral action minimizes the effects of disturbances and increases system stability.
3) Adaptability to process dynamics: PI compensators offer inherent adaptability to dynamic variations in the vaporizer process, such as changes in composition or heat transfer characteristics. Their proportional component facilitates rapid response to error changes, while the integral component allows control effort to be adjusted over time, ensuring consistent performance under varying conditions.
4) Overshoot and settling time control: Achieving precise control with minimal overshoot and settling time is essential to prevent oscillation and ensure efficient use of energy. PI compensators balance fast response (proportional action) with optimal steady-state error correction (integral action) to provide stable control without excessive oscillation.
5) Simplicity and ease of tuning: PI compensators have fewer adjustable parameters than complex strategies such as proportional-integral-derivative compensators or model-based approaches. This simplicity leads to easier tuning and implementation, reducing the risk of incorrect settings that could disrupt system behavior.
6) Robustness and reliability: PI compensators are well established and widely used due to their robustness to parameter variations, uncertainties, and sensor noise. This reliability ensures consistent control performance over time, contributing to stable and reliable operation.

- Drawbacks of PI compensators:
  1) Limited handling of complex dynamics: PI compensators may have difficulty handling highly nonlinear or time-varying processes that require more sophisticated control strategies. In such cases, advanced techniques such as model predictive control or adaptive control may provide better performance.
  2) Susceptibility to model mismatch: PI compensators rely on accurate process models for effective tuning. Model imprecision or changes in process behavior over time can lead to suboptimal control performance.
  3) Set point changes and large disturbances: While integral action compensates for steady-state errors, sudden large disturbances or set point changes can cause integral action to wind-up, resulting in overshoot or slow response until the accumulated error is resolved.
  4) Limited optimal performance for all scenarios: PI compensators are tuned for a specific range of operating conditions. Large changes in process dynamics or operating points can result in less than optimal control performance.

In summary, the adoption of PI compensators for the vaporizer process balances their well-established benefits in achieving accurate and stable control with their drawbacks in handling complex dynamics and varying scenarios. The selection meets the process requirements for steady-state accuracy, robustness, and ease of operation, while recognizing the need for careful tuning and consideration of potential limitations in certain scenarios.

The PI compensator designs related to the single loop control structure and the cascade loop control structure are presented below. From Figure 2, it can be seen that the single-loop control is labeled as LC based on the control of the level $h(t)$. On the other hand, the cascade loop is composed of a PC compensator (controls $P(t)$) and a TC (controls $T_s(t)$).

4.1 *LC Control Loop Design*

For the purpose of designing the LC compensator, the plant related to this control loop can be identified by considering Figure 3 and (15). The TF corresponds to the expression defined in (16).

$$G_{13}(s)=\frac{H(s)}{K_1(s)}=1.0272\cdot\frac{(s+3.161)}{(s+7.205\cdot10^{12})\cdot(s+1.38)} \tag{16}$$

According to [17,22], using an approximate model of (16) of the first-or-plus-dead-time (FOPDT) type, it is possible to design PI compensators using tables already developed for this purpose. Also according to [22], the use of a FOPDT approximation for TF modeling and subsequent PI compensator design offers several important advantages. First, FOPDT models are simple and interpretable, providing a compact representation of the system dynamics. This simplicity facilitates initial analysis and design. Second, FOPDT models often provide physical insight into the dominant time constants and dead-time behavior, improving the understanding of the system. In addition, parameter estimation is more straightforward due to fewer model parameters, useful when working with limited or noisy data. FOPDT approximations provide essential frequency-domain characteristics to assist in control design and stability analysis. These models act as a starting point for PI controller tuning, ensuring effective control and stability. The computational efficiency of FOPDTs is suitable for real-time control, and their applicability to industrial processes emphasizes their relevance. In addition, FOPDT models are valuable teaching tools that bridge theory and real-world applications.

Overall, FOPDT approximations offer a balance of simplicity, accuracy, and ease of use, providing a strong base for designing effective control systems while allowing a deeper understanding of the fundamental dynamics. For the reasons given above, the model in (16) is approximated to an FOPTD model. In (17), the model in (16) is defined in its canonical form [10].

$$G_{13}(s)=\frac{H(s)}{K_1(s)}=3.266\cdot10^{-13}\cdot\frac{(0.316\cdot s+1)}{(1.388\cdot10^{-13}\cdot s+1)\cdot(0.725\cdot s+1)} \tag{17}$$

From (17), the MATLAB procest command is applied, which is a part of the MATLAB system identification toolbox [23]. The MATLAB procest command is a powerful tool for identifying and modeling dynamic processes. It uses input-output data to estimate system dynamics by fitting models such as TFs or state-space models through optimization. It takes into account disturbances, noise, and time delays, enabling comprehensive system analysis and control design. First, a square-wave test signal is generated and used to stimulate (17). Next, a variable is formulated to simulate the output behavior of the model defined by (17). Once the procest command is performed, the approximate FODPT model is obtained as follows in (18). From here, the FOPTD parameters given by K_p = 3.2593×10^{-13}, the pole time constant τ_{p1} = 0.49975 s, and the dead time value τ_d = 0.0001 s are given.

sysFOPDT =

Process model with transfer function:

$$G(s)=\frac{K_p}{1+\tau_{p1}*s}*\exp(-\tau_d*s)$$

$$K_p=3.2593e^{-13}$$

$$\tau_{p1}=0.49975$$

$$\tau_d=0.0001$$

Parameterization: (18)

'P1D'

Number of free coefficients: 3

Use "getpvec", "getcov" for parameters and their uncertainties.

Status:

Estimated using PROCEST on time domain data "sys_iddata".

Fit to estimation data: 95.84%

To compare model (17) with model (18), the compare MATLAB command is used. This command generates a plot of both models showing the error between the two models in percent. This plot is shown in Figure 4a. From Figure 4a, it can be seen that the approximate model in (18) is quite close to the original model in (17). In fact, the error between the two models when excited by a square-wave test signal is close to 4.13 % (see equation (18)).

Finally, Figure 4b shows the step responses of the model in (17) and the model in (18). It can also be qualitatively verified that both curves are close, thus verifying that the approximation is proper.

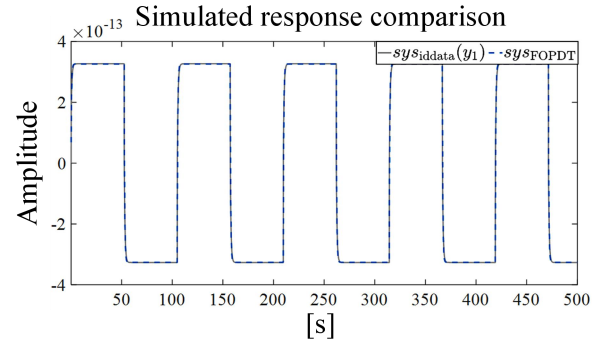

(a)

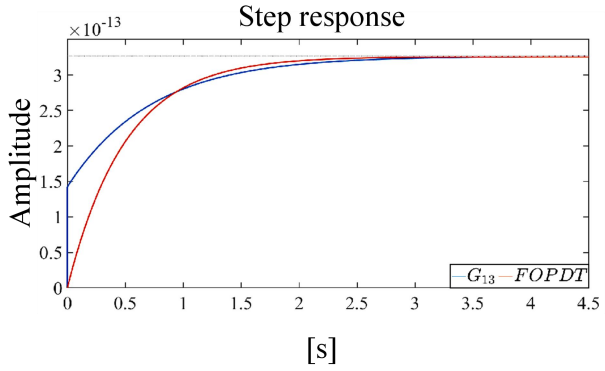

(b)

Figure 4. Dynamics under excitation of models (17) and (18). (a) Comparison of simulated responses based on (17) and (18). The error between the two models is 4.13 %. The sysiddata signal is the model in (17) in input/output object format. The sysFOPDT signal is the approximate model in (18). (b) Step response for models (17) and (18).

The next step is to tune the PI compensator. For this purpose, the transfer function $G_c(s)$ of the PI compensator in the s-domain is defined as follows

$$G_c(s) = \frac{k_c}{\tau_i} \cdot \frac{1+\tau_i \cdot s}{s} \tag{19}$$

Here, k_c and τ_i represent the tuning parameters of the compensator, which are the gain and the integral time (reset) of the compensator, respectively [10]. These parameters are determined using the off-line Ziegler-Nichols method [24] applied to processes represented by FOPTD models. This process follows a control diagram with a unitary feedback loop, as shown in Figure 5a. According to [24] and considering (18), the specific formula for calculating the tuning parameters of the compensator is derived as follows

$$\begin{cases} k_c = \dfrac{1}{K_p} \cdot \dfrac{\tau_{p_l}}{\tau_d} \\ \tau_i = 3.33 \cdot \tau_d \end{cases} \tag{20}$$

Evaluating (20), the values found for the tuning parameters are $k_c = 1.533 \cdot 10^{16}$ and $\tau_i = 3.33 \cdot 10^{-4}$ s. These initial values operate as a starting point for effective configuration of the PI compensator. However, it is important to note that these parameters are subject to refinement once the PI compensator is integrated into the system simulator, for example.

This tuning process involves fine-tuning k_c and τ_i by making incremental changes based on the system's response characteristics and desired performance criteria. Typically, manual iteration is used, where k_c and τ_i are adjusted incrementally in accordance with observed system behavior and target objectives [12,24].

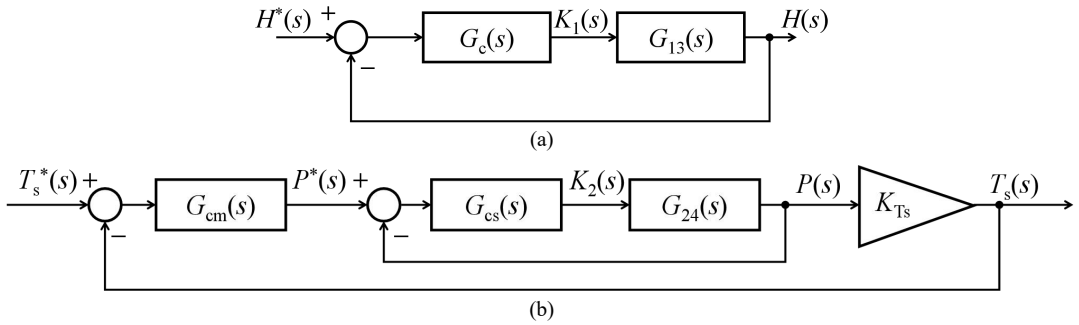

Figure 5. Block diagrams of the vaporizer control loops. (a) Control diagram of the level $h(t)$ built by a single feedback loop. (b) Cascade control loop regulating the temperature $T_s(t)$ and the pressure $P(t)$. The two control loops can be seen; the inner and the outer one.

4.2 *Design of the Cascade Control Loop*

To design the cascade control loop, the control diagram shown in Figure 5b is drawn, including an inner loop configured by the PI compensator $G_{cs}(s)$ (PC) and the plant $G_{24}(s)$, and an outer loop composed of the transfer function $P^*(s)/P(s)$, the gain K_{Ts}, and the PI compensator labeled $G_{cm}(s)$ (TC). From Figure 5b, the plant $G_{24}(s)$ is derived from the solution of (15), which is defined as follows

$$G_{24}(s)=\frac{P(s)}{K_2(s)}=0.0267\cdot\frac{\left(s+3.142\cdot10^{12}\right)}{\left(s+7.205\cdot10^{12}\right)\left(s+1.38\right)\left(s+0.012\right)} \tag{21}$$

Converting (21) to its canonical form, its new version is given as follows

$$G_{24}(s)=\frac{P(s)}{K_2(s)}=0.703\cdot\frac{\left(3.183\cdot10^{-13}\cdot s+1\right)}{\left(1.388\cdot10^{-13}\cdot s+1\right)\left(0.725\cdot s+1\right)\left(83.333\cdot s+1\right)} \tag{22}$$

Using a methodology similar to that used to derive (18), the analogous process is applied to the model defined in (22) to obtain its approximate FOPDT expression defined in (23), where the FOPTD parameters given by $K_p = 0.70326$, the pole time constant $\tau_{p1} = 83.457$ s, and the dead time value $\tau_d = 0.7161$ s are derived. Note that the error between the models (22) and (23) is comparatively smaller than the error between the expressions (17) and (18). This error is quantified to be 0.32 %, highlighting the close similarity in dynamics between models (22) and (23). Finally, Figure 6 shows the step responses of models (22) and (23). From Figure 6, the similarities of their dynamics can be verified again. Using the expressions presented in (19) and (20) and in accordance with the model given in (23) and [24], the tuning parameters for the compensator $G_{cs}(s)$ are derived. That is $k_c = 1.422$ and $\tau_i = 2.3846$ s.

sysFOPDT =

Process model with transfer function:

$$G(s)=\frac{K_p}{1+\tau_{p1}*s}*\exp\left(-\tau_d*s\right)$$

$$K_p=0.70326$$

$$\tau_{p1}=83.457$$

$$\tau_d=0.7161$$

Parameterization: (23)

'P1D'

Number of free coefficients: 3

Use "getpvec", "getcov" for parameters a nd their uncertainties.

Status:

Estimated using PROCEST on time domain d ata "sys_iddata_2".

Fit to estimation data: 99.68%

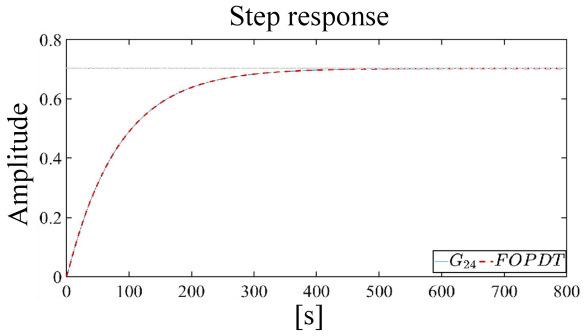

Figure 6. Step response for models (22) and (23).

Finally, based on expression (15) and considering Figure 3, a direct relationship between $P(s)$ and K_{Ts} can be established, which can be expressed as $P(s) \approx 0.125 \cdot T_s(s)$. This implies that $T_s(s) \approx 8 \cdot P(s)$, and therefore $K_{Ts} = 8$.

Using the information developed so far, it is possible to reduce the diagram shown in Figure 5b by applying the block reduction technique [10]. The reduced diagram of Figure 5b is shown in Figure 7.

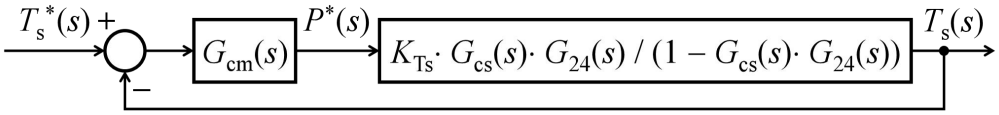

Figure 7. A simplified model of the block diagram shown in Figure 5b.

The $G_{cm}(s)$ compensator is designed using frequency techniques and the concept of phase margin (PM). Phase margin is a stability measure in control theory that evaluates a system's ability to handle disturbances. It quantifies the phase shift introduced by the system when the open-loop gain exceeds unity (0 dB). A higher phase margin means better stability and noise rejection, while a lower margin can lead to oscillations or instability. It is measured in degrees as the difference between 180° and the phase angle at unity gain frequency. Systems with a phase margin greater than 45°–60° are stable and robust, ensuring reliable performance [10,11,17].

As mentioned above, one of the key parameters in this design is the determination and adjustment of frequency (f_s) at which the compensator should be designed. To determine the f_s, the Bode diagram of the transfer function $P^*(s)/T_s(s)$ shown in Figure 7 is taken and plotted in Figure 8. It should be noted that, the expression for $G_{24}(s)$ using in Figure 7 corresponds to (22). From Figure 8, it can be seen that the crossover frequency (f_c) is approximately 0.22 Hz. This value of f_c is reasonable considering that the process involved is typically characterized by low-frequency dynamics, such as thermal and level processes [1,12]. Therefore, according to [10,11,17], a fs that is an order of magnitude smaller than f_c can be chosen to avoid potential frequency disturbances in the control elements. Thus, $f_s = f_c / 10$.

Based on Figure 7 and by removing the feedback path, the transfer function of the open-loop model is defined in as follows

$$G_{OL}(s) = \frac{k_{cm}}{\tau_{im}} \cdot \frac{1 + \tau_{im} \cdot s}{s} \cdot \frac{K_{T_s} \cdot G_{cs}(s) \cdot G_{24}(s)}{1 - G_{cs}(s) \cdot G_{24}(s)} \tag{24}$$

where k_{cm} and τ_{im} are the tuning parameters of the compensator $G_{cm}(s)$. It should be noted that in (24) the only unknown parameters are k_{cm} and τ_{im}, since the other TFs were already evaluated previously. Finally, the calculation of the parameters k_{cm} and τ_{im} are obtained by solving the system of equations defined in (25), where, $w_s = 2 \cdot \pi \cdot f_s$. Also, ϕ_{pm} is the angle of the PM, which in this case is set to 60°. The tuning parameters of the $G_{cm}(s)$ are derived and set to $k_{cm} \approx 0.08$ and $\tau_{im} \approx 0.01$.

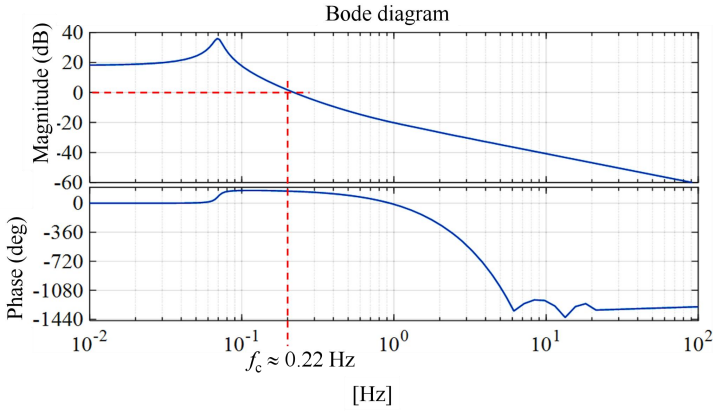

Figure 8. Bode diagram of the transfer function $P^*(s)/T_s(s)$ in open-loop. In this plot, $f_c \approx 0.22$ Hz.

$$\begin{cases} \text{abs}\left(G_{\text{OL}}\left(s\right)\right)\Big|_{s=\text{j}\cdot\omega_s} = 1 \\ \text{angle}\left(G_{\text{OL}}\left(s\right)\right)\Big|_{s=\text{j}\cdot\omega_s} = -180^{\circ} + \phi_{\text{PM}} \end{cases} \tag{25}$$

Thus far, the focus has been on developing compensators in the continuous time domain. Nevertheless, a significant determinative in control systems involves selecting between continuous and discrete compensators.

Continuous compensators have traditionally been more extensively used as they easily integrate with analog systems [25]. Nonetheless, they are subject to limitations. Their performance is affected by the physical constraints of analog hardware as they work in the analog domain [25]. The digital revolution has introduced discrete compensators as an alternative for digital control systems. Ideal for applications requiring precise real-time control and adaptability, these compensators use digital signal processing to enable rapid sampling, adaptive control, and advanced signal processing [26,27]. Nevertheless, they also present certain challenges, such as potential problems with sampling, quantization, and numerical stability [26,27]. The choice between continuous or discrete compensators depends on control system requirements and the underlying hardware. While continuous compensators have been established and are applicable for various functions, discrete compensators offer advantages for digital control and adaptability [26,27].

It is important to objectively evaluate the performance of compensators designed in continuous time versus those designed in discrete time, as previously noted. The discrete compensators are achieved through a method that converts their continuous time counterparts into discrete versions, as described in [28]. This conversion was performed using the MATLAB-Simulink control systems toolbox. The integral terms of the PI compensators are estimated with their bilinear form, using the trapezoidal method. A sampling time of 0.1 seconds was specified for the design. The tuning parameters of each compensator were adjusted through heuristics by trial and error. Table 6 displays these tuning parameters.

Table 6. Tuning Parameters of the Vaporizer Digital Compensators

Compensator	Tuning parameter	Value
$G_c(s)$	k_c	72.144
	t_i	0.028
$G_{cs}(s)$	k_c	0.174
	t_i	18
$G_{cm}(s)$	k_c	3.239
	t_i	33.051

This section discusses the design of a control system for a vaporizer process using both single-loop and cascade control structures. The single-loop approach focuses on maintaining a steady liquid level, while the cascade structure addresses the complex relationship between temperature and pressure. The mathematical model of the control system is translated to the Laplace domain, allowing PI compensators to be designed using FOPTD approximations. Cascade loop design utilizes frequency techniques and PM considerations. The design process carefully weighs the advantages and disadvantages of PI compensators and effectively utilizes the advantages of cascade control. The result is a comprehensive control strategy that increases the stability and control of the vaporizer process.

5. Simulation Results

The simulation results utilized the MATLAB-Simulink platform to model and evaluate the system defined by (10) and (11), using values from Table 4 and Table 5. The outcomes displayed in Figure 9 and 10 provide valuable insights into the transient behaviors of variables related to both continuous-time compensators ($h_c(t)$, $T_{sc}(t)$, and $P_c(t)$) and discrete-time compensators ($h_d(t)$, $T_{sd}(t)$, and $P_d(t)$). Additionally, the analysis in Figure 11 examines $k_{1c}(t)$, $k_{1d}(t)$, $k_{2c}(t)$, and $k_{2d}(t)$ dynamics.

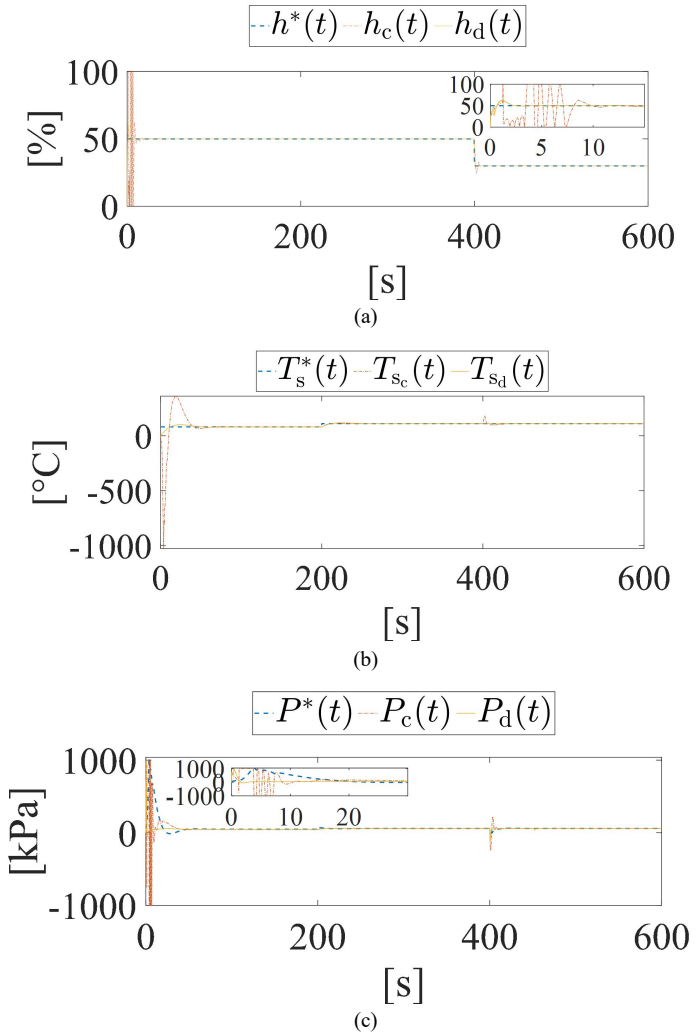

Figure 9. Simulation results under transient operation of the process taking place in the vaporizer. Reference values $h^*(t)$ = 50 %, and $T_s^*(t)$ = 80 °C. Step change in $T_s(t)$ and $h(t)$ at 200 s and 400 s respectively. (a). Dynamic of $h_c(t)$ and $h_d(t)$. (b) Dynamic of $T_{sc}(t)$ and $T_{sd}(t)$. (c) Dynamic of $P_c(t)$ and $P_d(t)$

In the subsequent analysis, the generic dynamics of the variables displayed in Figure 9–Figure 11 will be studied without specifying their origin from continuous or discrete compensators. During the initial stages of the system when both valves are fully closed, specific setpoints were established at $h(t)$ = 50 % and $T_s(t)$ = 80°C. Based on the simulation results in Figure 9, $h(t)$, $T_s(t)$, and $P(t)$ steadily converge to their desired values, with precise values of 50 %, 47.22 kPa, and 80°C at 20 s, 100 s, and 120 s, respectively. Similarly, it can be observed from Figure 10 that both $f_i(t)$ and $w_s(t)$ attain their steady-state levels at 92.246 s and 124.665 s, with values of 45.31 m3/s and 16.59 kg/s, respectively. Furthermore, Figure 11 demonstrates that $k_1(t)$ and $k_2(t)$ also reach their steady-state positions at 126.954 s and 150 s, respectively, with values of 0.613 pu (61.3 %) and 0.421 pu (42.1 %).

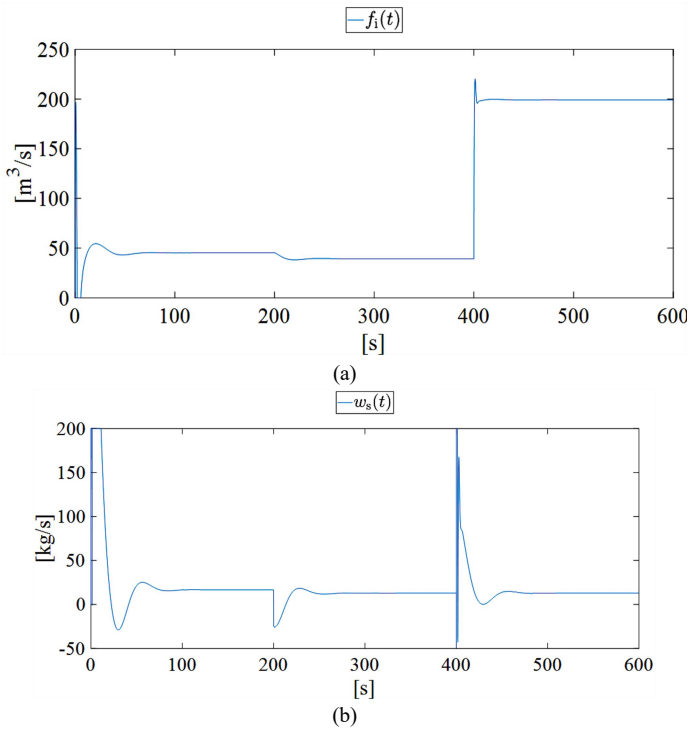

Figure 10. Simulation results under transient operation of the process taking place in the vaporizer. Reference values $h^*(t) = 50$ %, and $T_s^*(t) = 80$ °C. Step change in $T_s(t)$ and $h(t)$ at 200 s and 400 s respectively. Dynamic of $f_i(t)$. (b) Dynamic of $w_s(t)$.

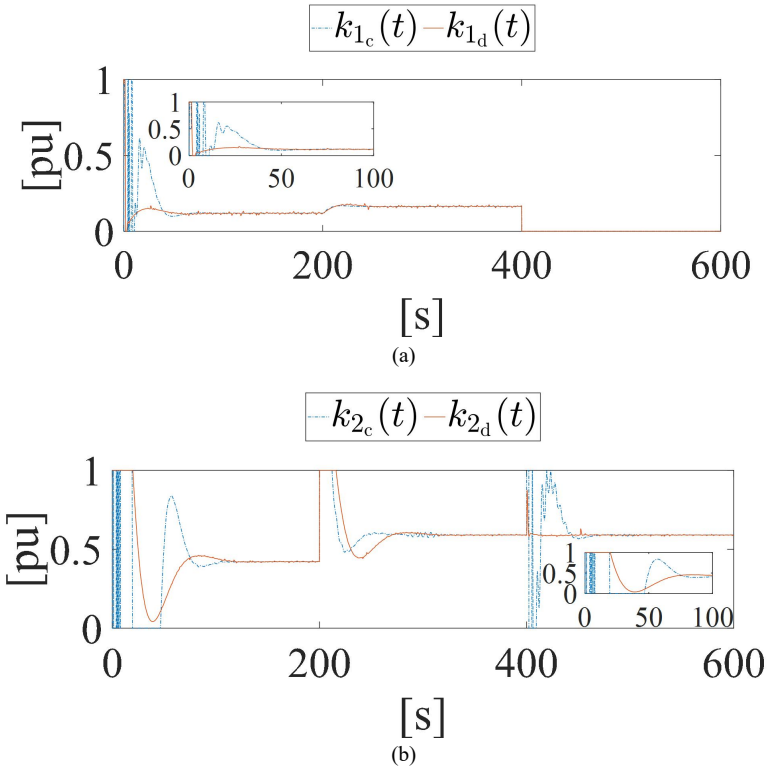

Figure 11. Simulation results under transient operation of the process taking place in the vaporizer. Reference values $h^*(t) = 50$ %, and $T_s^*(t) = 80$ °C. Step change in $T_s(t)$ and $h(t)$ at 200 s and 400 s respectively. (a) Dynamic of $k_{1c}(t)$ and $k_{1d}(t)$. (b) Dynamic of $k_{2c}(t)$ and $k_{2d}(t)$.

At 200 s, a perturbation is introduced in $T_s(t)$, which changes it to 60°C and then stabilizes around this value for about 274 s. This perturbation has a ripple effect on $f_i(t)$ and $w_s(t)$, which both experience a decrease. This decrease can be attributed to the fact that the temperature change affects the efficiency of the evaporation process, requiring adjustments in $f_i(t)$ and $w_s(t)$. These changes are reflected in the $k_1(t)$ and $k_2(t)$ positions,

where $k_2(t)$ goes through a complete cycle from full closure to full opening before returning to its pre-disturbance level at 562.3 s.

Then, at 400 s, another perturbation affects $h(t)$, increasing it to 80% at 450 s. The perturbation affects variables such as $T_s(t)$, $P(t)$, $w_s(t)$, and $f_i(t)$. While $T_s(t)$ is disturbed, it returns to its pre-disturbance steady state value. The $P(t)$ experiences a similar perturbation, but stabilizes at 47.22 kPa before the perturbation. Notably, the behavior of the system during this perturbation appears more pronounced, particularly in $T_s(t)$, indicating its effect on the energy and mass balances. The flow variable $f_i(t)$ stabilizes at a new value of 200 m^3/s, significantly higher than its initial value of 39.25 m^3/s.

Analyzing the data presented in Figure 9 and Figure 11, it is clear that the variables controlled by discrete compensators show superior performance in terms of the defined FoM, specifically overshoot (OS) and steady-state error (SE). The values in Table 7 confirm that $h_d(t)$, $T_{sd}(t)$, and $P_d(t)$ consistently exhibit significantly lower FoM values compared to their continuous-time counterparts ($h_c(t)$, $T_{sc}(t)$, and $P_c(t)$).

Table 7. Summary of FoMs, i.e., OS and SE regarding operation of the Vaporizer

Time [s]	FoM	Variables	Value [%]	Variables	Value [%]
Start-up	OS	$h_c(t)$	15	$h_d(t)$	5.5
		$T_{sc}(t)$	20	$T_{sd}(t)$	2.2
		$P_c(t)$	25	$P_d(t)$	7.8
	SE	$h_c(t)$	~0	$h_d(t)$	~0
		$T_{sc}(t)$	~0	$T_{sd}(t)$	~0
		$P_c(t)$	~0	$P_d(t)$	~0
200	OS	$h_c(t)$	4.3	$h_d(t)$	-
		$T_{sc}(t)$	-	$T_{sd}(t)$	-
		$P_c(t)$	3.5	$P_d(t)$	-
	SE	$h_c(t)$	~0	$h_d(t)$	~0
		$T_{sc}(t)$	~0	$T_{sd}(t)$	~0
		$P_c(t)$	~0	$P_d(t)$	~0
400	OS	$h_c(t)$	5.6	$h_d(t)$	2.9
		$T_{sc}(t)$	3.5	$T_{sd}(t)$	-
		$P_c(t)$	23	$P_d(t)$	12.8
	SE	$h_c(t)$	~0	$h_d(t)$	~0
		$T_{sc}(t)$	~0	$T_{sd}(t)$	~0
		$P_c(t)$	~0	$P_d(t)$	~0

The implication is that the system's discrete compensators result in lower OS, which is a significant advantage. Furthermore, in the 200 second, the OS of variables such as $h_c(t)$ and $P_c(t)$ improves significantly, and $T_{sc}(t)$ even eliminates the OS altogether. Most importantly, $h_d(t)$, $T_{sd}(t)$, and $P_d(t)$ show remarkable reductions in SE, further demonstrating their superior performance. Throughout, minimal SE values reinforce the system's rapid stabilization around set points.

Although the system does not fully meet the specified constraints on OS and SE, where the values should not exceed 5 % and 1 %, respectively, the system begins to meet the OS requirements after the system change at 200 s, while SE remains consistently well below the defined constraint. This is true for all variables ($h_i(t)$, $T_{si}(t)$, and $P_i(t)$, where $i \in \{c, d\}$). These results highlight the potential for further optimization to minimize the initial overshoot during system startup and to fine-tune system performance to meet even more stringent settling error targets.

In conclusion, the simulation results highlight the effectiveness of the designed compensators in achieving stable and responsive control in the vaporizer process, and in particular, the superiority of discrete-time compensators in terms of overshoot and settling error.

6. Conclusions

In this thoroughly designed and rigorously reviewed study, a comprehensive analysis of a vaporizer process and its control system is presented. The introduction provides a fundamental understanding of vaporizer systems' importance in industrial applications and the critical requirement for advanced control strategies to achieve efficiency and stability. The vaporization process description describes the complexities of the vaporization process, highlighting critical parameters such as liquid level, temperature, and pressure that require precise control for optimal performance.

The process modeling section provided the foundation for the subsequent control system design. Complex mathematical formulations (equations (10) and (11)) and data from Tables 4 and 5 played a vital role in

formulating the models. The detailed outline of the vaporization process framework included continuous-time compensators ($h_c(t)$, $T_{sc}(t)$, and $P_c(t)$) as well as discrete-time compensators ($h_d(t)$, $T_{sd}(t)$, and $P_d(t)$). This framework laid the foundation for the central focus of this study: control system design.

The design of the control system was based on a thorough comprehension of process dynamics, leading to the development of compensators that demonstrated accuracy in maintaining setpoints as well as resilience against perturbations. The use of the MATLAB-Simulink platform for simulations provided significant insights into the transient behaviors of these variables. The control system's ability to direct the process towards desired conditions while withstanding perturbations like temperature and liquid level changes demonstrated its efficacy.

One of the key findings was the significant advantages provided by the discrete-time compensators ($h_d(t)$, $T_{sd}(t)$, and $P_d(t)$) in terms of critical performance metrics, particularly overshoot and steady-state error. The findings in Table 6 confirm that discrete-time compensators consistently perform better than their continuous-time counterparts. This advantage arises from the reduced overshoot in discrete compensators, which improves the overall system stability. Additionally, the substantial reduction in steady-state error results in a faster convergence of the system to setpoints.

Although the system did not entirely satisfy the predefined constraints regarding overshoot and settling error, where values should not exceed 5 % and 1 %, respectively, there was a noticeable improvement in overshoot after the system changes at 200 seconds. The steady-state error consistently remained low, indicating promising opportunities for continued optimization.

The study's conclusion emphasizes the strong effectiveness of the designed compensators in achieving stability and responsiveness in the vaporization process. Additionally, it highlights the superior performance of discrete-time compensators in minimizing overshoot and settling errors. This work provides a strong foundation for future improvements and optimizations to meet more challenging control objectives and ensure process reliability in industrial applications.

Conflict of Interest

There is no conflict of interest for this study.

References

[1] Luyben, W.L. *Process Modeling, Simulation and Control for Chemical Engineers*. Subsequent edition. Mc Graw-Hill College: New York, NY, USA, 1989; ISBN: 978-0-07-039159-8.

[2] Bralla, J.G. *Handbook of Manufacturing Processes - How Products, Components and Materials Are Made*. First Edition. Industrial Press, Inc.: New York, NY, USA, 2007; ISBN: 978-0-8311-3179-1.

[3] Alexandrov, D.V.; Alexandrova, I.V.; Ivanov, A.A. Mathematical modeling of vaporization process for a p olydisperse ensemble of liquid drops. *Math. Methods Appl. Sci.* **2020**, *44*, 12101–12107, https://doi.org/10.1002/mma.6749.

[4] Sarip, M.S.M. *Model Predictive Control of Vaporizer in Vinyl Acetate Monomer Process*. Master's thesis, U niversity Malaysia Pahang, Gambang, Malaysia, May 2008.

[5] Yu, K.; Sun, J.; Yin, J. Modeling and analysis of heat transfer in submerged combustion vaporizer under supercritical pressure. *Cryogenics* **2021**, *116*, 103287, https://doi.org/10.1016/j.cryogenics.2021.103287.

[6] Sun, B.; Wadnerkar, D.; Utikar, R.P.; Tade, M.O.; Kavanagh, N.; Faka, S.; Evans, G.M.; Pareek, V.K. Modeling of Cryogenic Liquefied Natural Gas Ambient Air Vaporizers. *Ind. Eng. Chem. Res.* **2018**, *57*, 9281–9291, https://doi.org/10.1021/acs.iecr.8b01226.

[7] Zhu, Y.; Li, T.; Xia, C.; Feng, Y.; Zhou, S. Simulation analysis on vaporizer/mixer performance of the high-pressure SCR system in a marine diesel. *Chem. Eng. Process. - Process. Intensif.* **2020**, *148*, 107819, https://doi.org/10.1016/j.cep.2020.107819.

[8] Huang, K.; Zhou, X.; Huang, C.; Wang, L.; Li, D.; Zhao, J. Heat Transfer Analysis and Operation Optimiza tion of an Intermediate Fluid Vaporizer. *Energies* **2023**, *16*, 1383, https://doi.org/10.3390/en16031383.

[9] Li, S.; Ju, Y. Review of the LNG intermediate fluid vaporizer and its heat transfer characteristics. *Front. Energy* **2021**, *16*, 429–444, https://doi.org/10.1007/s11708-021-0747-y.

[10] Ogata, K. *Modern Control Engineering*. 5th edition. Pearson: Boston, MA, USA, 2009; ISBN: 978-0-13-615673-4.

[11] Kuo, B.C. *Automatic Control Systems*. 6th edition. Prentice Hall: Englewood Cliffs, NJ, USA, 1991; ISBN: 978-0-13-051046-4.
[12] Smith, C.A.; Corripio, A.B. *Principles and Practice of Automatic Process Control.* 2nd Edition. Wiley: New York, NY, USA, 1997; ISBN 978-0-471-57588-7.
[13] Campos-Salazar, J.M. Design of a Linear-Quadratic Regulator for the Control of an Oil-Heating Tank. Modeling and Simulation. *J. Math. Techn. Comput. Math.* **2023**, *2*, 337–346.
[14] Packard, M.H.; Stoltzfus, D. Evaluation of Methodology for LPG Fuel System Integrity Tank Test. *NREL*, https://doi.org/10.2172/1766850.
[15] Valve Sizing Calculation (Traditional Method). Available online: www.emerson.com/documents/automation/manual-valve-sizing-standardized-method-fisher-en-140724.pdf (access on 10 August 2023).
[16] AMERICAN NATIONAL STANDARD, ANSI/ISA-5.1-2009, Instrumentation Symbols and Identification. Available online: http://integrated.cc/cse/Instrumentation_Symbols_and_Identification.pdf (access on 10 August 2023)
[17] Levine, W.S. The Control Handbook (Three Volume Set). CRC Press: Boca Raton, FL, USA, 2018; ISBN: 978-1-315-21869-4.
[18] Campos-Salazar, J.M.; Lecaros, P.; Sandoval, R. Dynamic Analysis and Performance Comparison of Linear and Nonlinear Controllers Applied to a Nonlinear Non-Interacting and Interacting Process. *TechRxiv*.
[19] Devan, P.A.M.; Hussin, F.A.; Ibrahim, R.; Bingi, K.; Abdulrab, H. Fractional-Order Predictive PI Controller for Process Plants with Deadtime. In Proceedings of 2020 IEEE 8th R10 Humanitarian Technology Conference (R10-HTC), Kuching, Malaysia, 1–3 December 2020, https://doi.org/10.1109/R10-HTC49770.2020.9357000.
[20] Briones, O.; Rojas, A.; Sbarbaro, D. Generalized Predictive PI Controller: Analysis and Design for Time Delay Systems. In Proceedings of 2021 American Control Conference (ACC), New Orleans, LA, USA, 25–28 May 2021, https://doi.org/10.23919/ACC50511.2021.9482789.
[21] Bensaoud, O.; Tokhmechi, A.; Sargeant, N. Comparison of PI, GMC and DMC Control For Reactor/Flash Unit Process. In Proceedings of the 2021 IEEE 1st International Maghreb Meeting of the Conference on Sciences and Techniques of Automatic Control and Computer Engineering MI-STA; Tripoli, Libya, 25–27 May 2021, https://doi.org/10.1109/MI-STA52233.2021.9464513; pp. 7–12.
[22] Júnior, G.A.; dos Santos, J.B.; Barros, P.R. On Simple Identification Techniques for First-Order plus Time-Delay Systems. **2009**, *42*, 605–610, https://doi.org/10.3182/20090706-3-fr-2004.00100.
[23] Ljung, L. *System Identification Toolbox for Use with MATLAB: User's Guide: Version 4*. MathWorks, Inc: Natick, MA, USA, 1997.
[24] Ho, W.; Hang, C.; Zhou, J. Performance and gain and phase margins of well-known PI tuning formulas. *IEEE Trans. Control. Syst. Technol.* **1995**, *3*, 245–248, https://doi.org/10.1109/87.388135.
[25] Ogata, K. *Discrete-Time Control Systems; 2nd edition*. Pearson: Englewood Cliffs, NJ, USA, 1995; ISBN: 978-0-13-034281-2.
[26] Abidi, K.; Xu, J.-X. Studies in Systems, Decision and Control. In *Advanced Discrete-Time Control: Designs and Applications*. Springer: Singapore, Singapore, 2015; ISBN: 978-981-287-477-1.
[27] Zarrop, M.B. Book Review: Analysis and Design of Discrete Linear Control Systems. *Int. J. Electr. Eng. Educ.* **1994**, *31*, 85–85, https://doi.org/10.1177/002072099403100109.
[28] Phillips, C.L.; Nagle, H.T. *Digital Control System Analysis and Design; Subsequent edition*. Prentice Hall: Englewood Cliffs, NJ, USA, 1994; ISBN: 978-0-13-309832-7.